Electronic Supplementary Information

Glycerol oxidation assisted electrocatalytic nitrogen reduction: ammonia and glyceraldehyde co-production on bimetallic RhCu ultrathin nanoflakes nanoaggregates

Juan Bai,[a,‡] Hao Huang,[b,‡] Fu-Min Li,[b] Yue Zhao,[a] Pei Chen,[a] Pu-Jun Jin,[a] Shu-Ni Li,[b] Hong-Chang Yao,[c] Jing-Hui Zeng[a] and Yu Chen*[,a]

[a] Key Laboratory of Macromolecular Science of Shaanxi Province, Key Laboratory of Applied Surface and Colloid Chemistry (MOE), Shaanxi Key Laboratory for Advanced Energy Devices, School of Materials Science and Engineering, Shaanxi Normal University, Xi'an 710062, China.
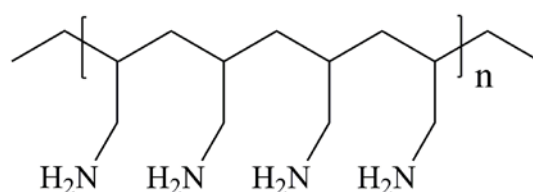
E-mail: ndchenyu@gmail.com (Y. Chen)

[b] School of Chemistry and Chemical Engineering, Shaanxi Normal University, Xi'an 710062, PR China.

[c] College of Chemistry and Molecular Engineering, Zhengzhou University, Zhengzhou 450001, PR China.

‡ J. Bai and H. Huang contributed equally to this work.
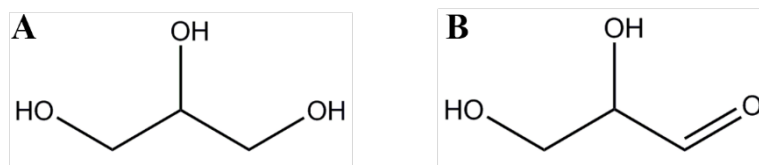
Scheme S1. The molecular structure of (A) glycerol and (B) glyceraldehyde.

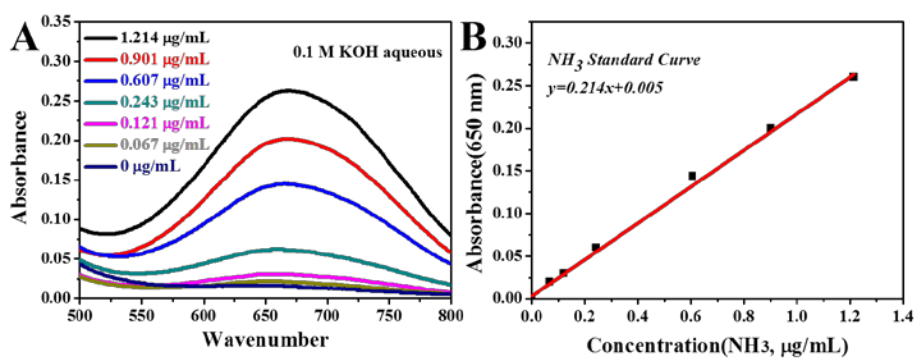**Scheme S2.** The molecular structure of polyallylamine hydrochloride.

Fig. S1 Absolute calibration of the phenate method using ammonium solutions of known concentration as standards. (A) UV-Vis curves of phenate assays after in darkness for 3 hours at room temperature, (B) calibration curve used for estimation of NH_3 by NH_4^+ ion concentration. The absorbance at 655 nm was measured by UV-Vis spectrophotometer, and the fitting curve shows good linear relation of absorbance with NH_4^+ ion concentration ($y = 0.214x + 0.005$) of three times independent calibration curves.
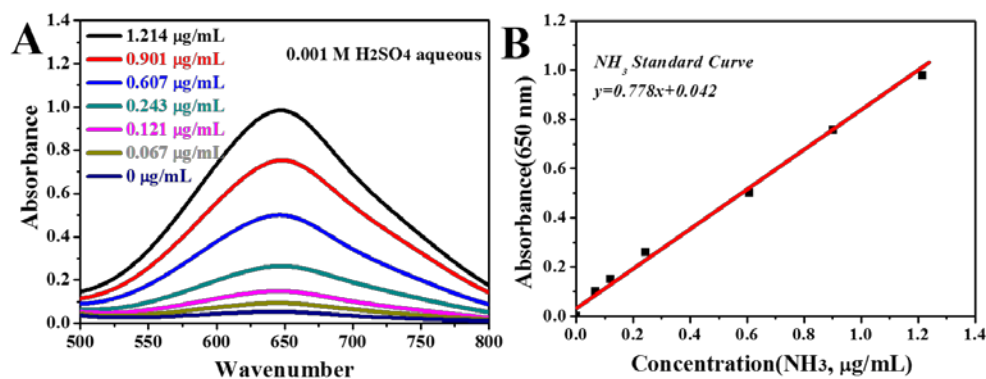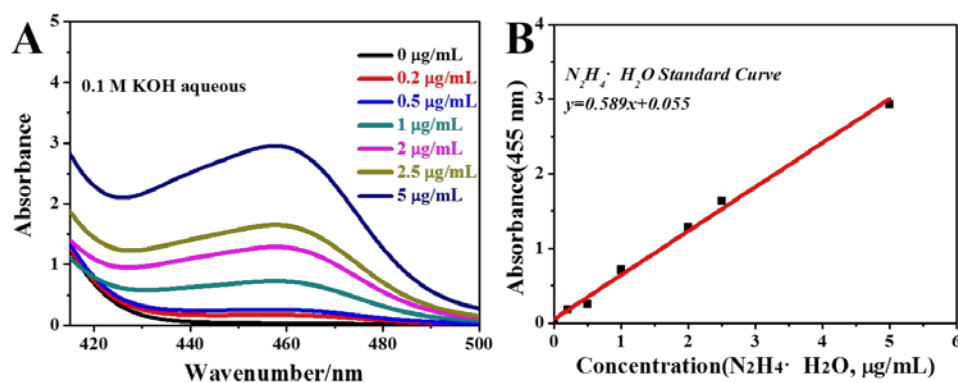
Fig. S2 Absolute calibration of the phenate method using ammonium solutions of known concentration as standards. (A) UV-Vis curves of phenate assays after in darkness for 3 hours at room temperature, (B) calibration curve used for estimation of NH_3 by NH_4^+ ion concentration. The absorbance at 655 nm was measured by UV-Vis spectrophotometer, and the fitting curve shows good linear relation of absorbance with NH_4^+ ion concentration (y =0.778x + 0.042) of three times independent calibration curves.

Fig. S3 Absolute calibration of the Watt and Chrisp (para-dimethylamino-benzaldehyde) method for estimating $N_2H_4 \cdot H_2O$ concentration, using $N_2H_4 \cdot H_2O$ solutions of known concentration as standards. (A) UV-Vis curves of various $N_2H_4 \cdot H_2O$ concentration after incubated for 10 min at room temperature, (B) calibration curve used for estimation of $N_2H_4 \cdot H_2O$ concentration. The absorbance at 455 nm was measured by UV-Vis spectrophotometer, and the fitting curve shows

good linear relation of absorbance with $N_2H_4 \cdot H_2O$ concentration (y = 0.589x+0.055) of three times independent calibration curves.
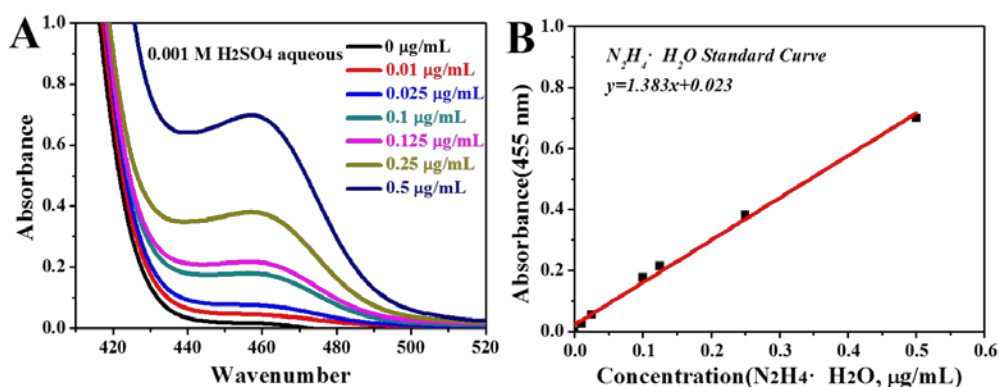

Fig. S4 Absolute calibration of the Watt and Chrisp (para-dimethylamino-benzaldehyde) method for estimating $N_2H_4 \cdot H_2O$ concentration, using $N_2H_4 \cdot H_2O$ solutions of known concentration as standards. (A) UV-Vis curves of various $N_2H_4 \cdot H_2O$ concentration after incubated for 10 min at room temperature, (B) calibration curve used for estimation of $N_2H_4 \cdot H_2O$ concentration. The absorbance at 455 nm was measured by UV-Vis spectrophotometer, and the fitting curve shows good linear relation of absorbance with $N_2H_4 \cdot H_2O$ concentration (y = 1.383x+0.023) of three times independent calibration curves.
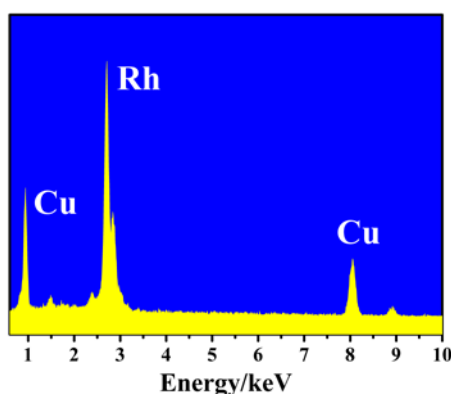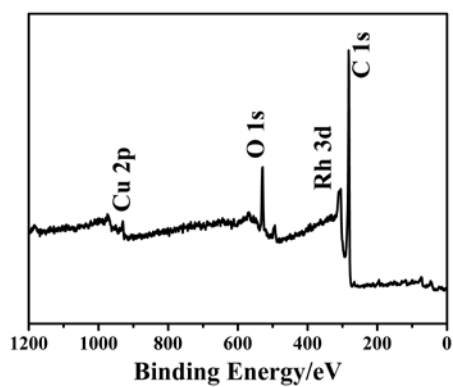

Fig. S5 EDX spectrum of RhCu-BUNNs.

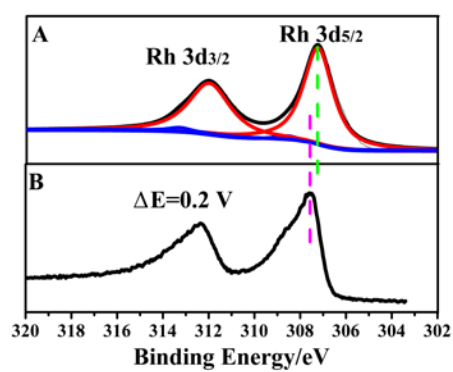**Fig. S6** XPS survey spectrum of RhCu-BUNNs.

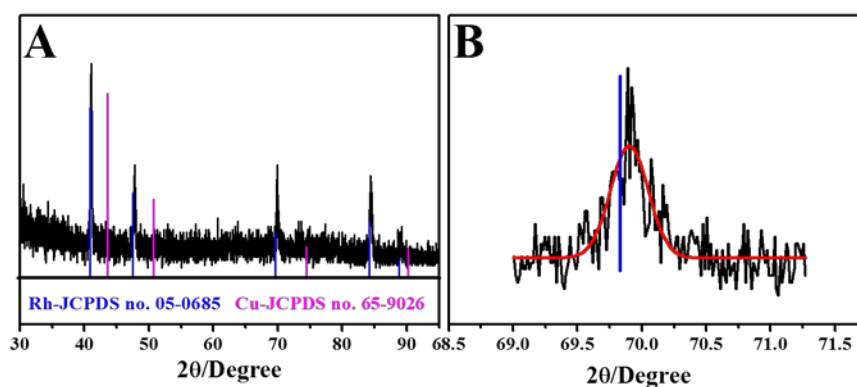**Fig. S7** Rh 3d XPS spectra of (A) RhCu-BUNNs and (B) Rh-UNNs.

Fig. S8 (A) XRD spectrum of RhCu-BUNNs after the calcination at 600 °C, (B) Enlarged XRD pattern.

Fig. S9 Photographs of mixture of $CuCl_2$ + polyallylamine hydrochloride + HCHO (A) before and (B) after heating for 6 h at 140 °C.
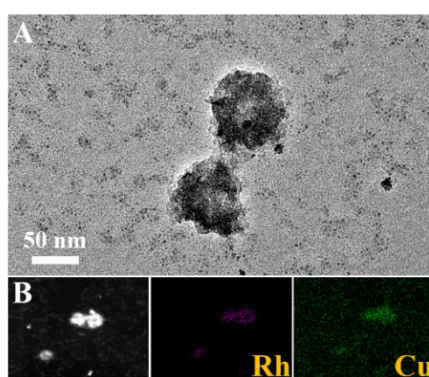

Fig. S10 (A) TEM image, (B) EDX mapping of the obtained products after increasing the amount of Cu^{II} precursor to Rh^{III}/Cu^{II}=2:1. As observed, TEM image show an obvious phase separation, in which a large number of tiny nanocrystals are observed (Figure S6 A). Further EDX mapping analysis confirm that these tiny nanocrystals are Cu nanocrystals (Figure S6 B).
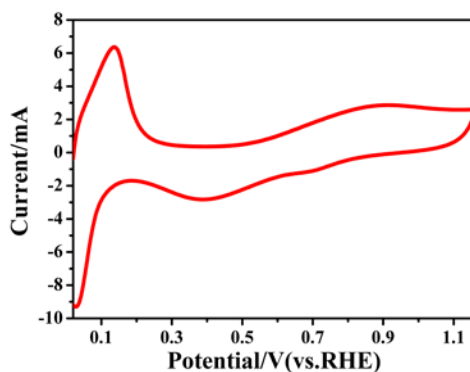

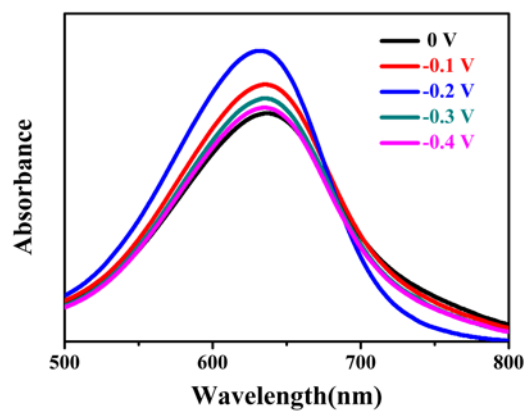**Fig. S11** CV curve of RhCu-BUNNs in Ar-saturated 0.5 M H_2SO_4 solution at 50 mV s^{-1}.

Fig. S12 UV-Vis absorption spectra of the electrolytes after electrolysis stained with indophenol indicator.
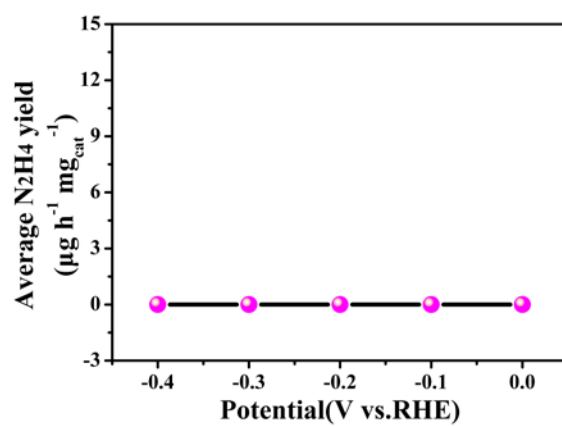

Fig. S13 $N_2H_4 \cdot H_2O$ yield rate at each given potentials.
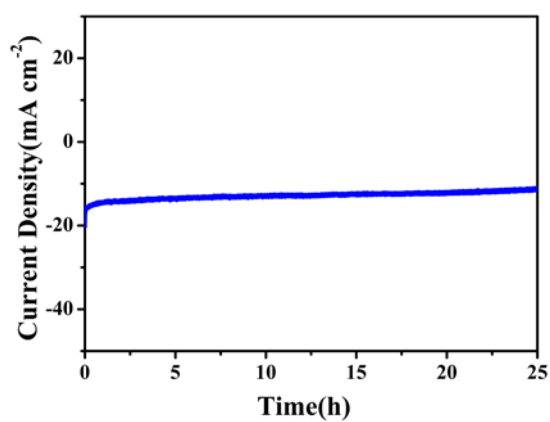

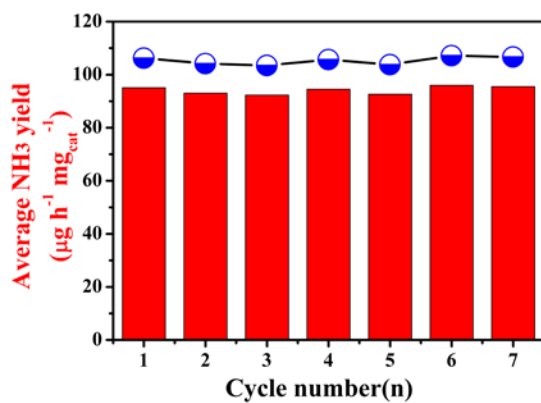**Fig. S14** Chronoamperometric curve of RhCu-BUNNs in 0.1 M KOH solution at -0.2 V potential for 25 h.

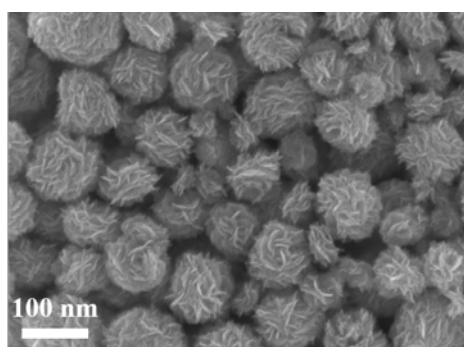**Fig. S15** Recycling test of RhCu-BUNNs. at the potential of −0.2 V.

Fig. S16 SEM image of RhCu-BUNNs after the long-term chronoamperometry.
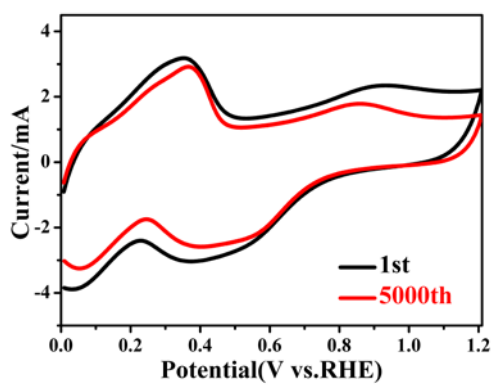

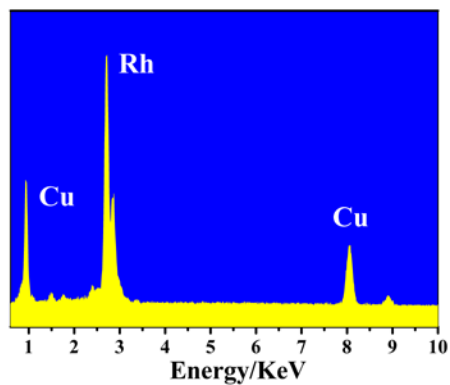**Fig. S17** The continuous CV curves of RhCu-BUNNs in Ar-saturated 0.1 M KOH solution at 50 mV s^{-1}.

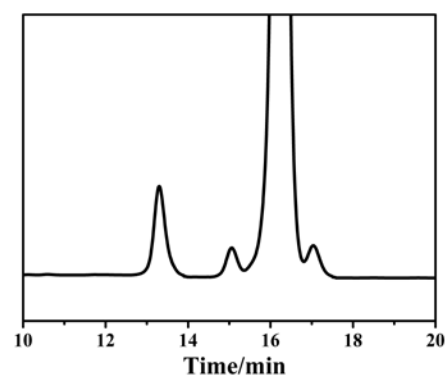**Fig. S18** EDX spectrum of RhCu-BUNNs after GOR.

Fig. S19 HPLC chromatogram of the product obtained from the GOR cell in three-electrode system.
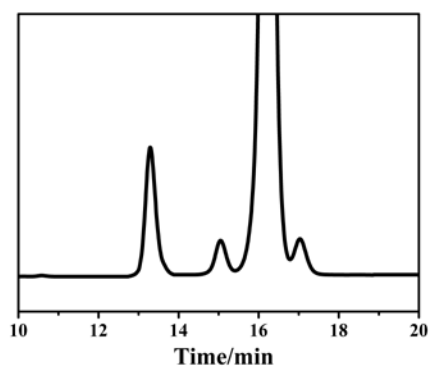

Fig. S20 The HPLC chromatogram of the product obtained from the GOR cell in two-electrode system.